RSC Advances

PAPER

View Article Online
View Journal | View Issue

Cite this: *RSC Adv.*, 2020, **10**, 44323

A photo-reversible crosslinking resin for additive manufacturing: reversibility and performance

Hanyu Xue, *[ab] Xinzhong Li,[ab] Jianrong Xia *[ab] and Qi Lin*[ab]

Received 30th July 2020
Accepted 3rd December 2020

DOI: 10.1039/d0ra06587k

rsc.li/rsc-advances

Improving the adhesion between layers and achieving the recycling of resins are challenges in additive manufacturing (AM) technology. In this work, a new type of photo-reversible crosslinking resin based on polyvinyl alcohol (PVA) and coumarin (HMC) was prepared *via* grafting reaction. The critical idea was to create a coumarin based photo-reversible crosslinking resin by carefully tailoring the photo-crosslinking time and temperature, so that the resin could be extruded through the nozzle and then maintain the proper shape during UV-curing. Photo-reversible crosslinking of AM resin was realized without the use of monomers, photo-initiators or propagating. A reasonable irradiation time with 354 nm (crosslink) or 254 nm UV light (cleavage) of 10 min was critical for photo-reversible crosslinking of PVA-*g*-HMC at 120 °C. An important result of this work was that the developed photo-reversible crosslinked resin could be reused and the printed resin exhibits excellent adhesion properties, thermal conductivity and oxygen barrier performance.

1. Introduction

Additive manufacturing (AM, as 3D printing is called) shows a great advantage as an advanced manufacturing technique for many applications, including biomedical, mechanical engineering and articles for daily use.[1,2] Fused deposition modeling (FDM) prints 3D objects using thermoplastic resins as raw materials,[3] which are directly deposited to a warm up platform through a three dimensional moving nozzle. Specifically, a thermoplastic printed layer is deposited in the plane parallel to the previous surface, therefore polymer chains have a low degree of association between layers so the bonding strength between the layers is limited.[4] This problem also appeared in stereolithographic (SLA) 3D printing, which is also an additive manufacturing method that creates prints layer by layer. Compared with FDM techniques, a high resolution could be achieved by using SLA-based techniques. However, the crosslinking of photo-polymer led to a rigid and brittle structure.[5–7]

Crosslinking the molecular chains between layers was one of the effective ways to improve the final properties of AM materials.[8] While recycling approaches was urgently required for AM materials in view of increasing processing wastes during printing.[9] As the spatial and temporal application of rays could easily be controlled, photo-responsive crosslinking drew wide attention.[10–13] Coumarin was a typical photo-responsive functional molecule, which was a [2 + 2] cycloaddition under an UV irradiation of 354 nm, while the photo-degradation reversed upon exposure to an UV light of 254 nm. Therefore, polymers which were crosslinked by coumarin could be reversible crosslinking functionalized.[14–19] In the work of Govindarajan, S. R., a hydrophilic coumarin-PEG polyester (CPP) for 3D printing was described. The CPP was viscoelastic and could be printed into layer-by-layer patterns.at room temperature. Under an UV irradiation of 354 nm, the coumarin groups in the side chain of CPP occurred [2 + 2] photo-cyclization which form a polymer network without using monomers, photo-initiators or propagating.[12] In the further study, it was found that the photo-reversible reaction of coumarin group could be easily realized in solution, but in solid state, especially in crystal, the photo-reversibility of coumarin group was weakened. This was because the photo-reversible properties of coumarins follow the top chemical rules. When the distance between two coumarin groups was less than 4.2 μ and they were arranged in parallel, the photo-degradation could be carried out.[20–24] Dynamic covalent networks of intrinsic bond exchange reactions such as disulfide crosslinks[7] and Diels–Alder (DA) systems also applied.[25,26] However, recyclable soft-matter did not meet the actual requirements, especially mechanical properties.

Design of a photo-reversible crosslink AM resin provides an opportunity to achieve the recycling of AM thermosets and improve the bonding strength between the layers, which was not possible for conventional polymers. In this work, a new type of photo-reversible crosslinking resin based on polyvinyl alcohol (PVA) and coumarin (HMC) was prepared *via* grafting reaction, while a AM technique to improve the bonding strength between the layers was reported.

[a]*Fujian Engineering and Reaearch Center of New Chinese Lacquer Materials, Ocean College, Minjiang University, Fuzhou, Fujian 354108, PR China. E-mail: 366157115@qq.com; jrxia@mju.edu.cn; qlin1990@163.com*

[b]*Fujian Provincial University Engineering Research Center of Green Materials and Chemical Engineering, Minjiang University, Fuzhou, Fujian 354108, PR China*

2. Materials and reagents

2.1. Materials and reagents

Poly(vinyl alcohol) 1799 (PVA, alcoholysis degree 98–99%), 7-hydroxy-4 methylcoumarin (AR, 98%), bromoacetic acid (AR, 99%) and dith butyl dilaurate (CP, 95%) were purchased from Aladdin Chemical Reagent Co, Ltd Shanghai, China. Potassium acetate (99.0%), *N*,*N*′-dimethylformamide (DMF, 99.5%), *N*,*N*′-dicyclohexycarbodiimide (DCC, 99%) and ethyl acetate (99.0%) were obtained from Sinopharm Chemical Reagent Co, Ltd Shanghai, China.

2.2. Preparation of 2-(4-methyl-2-oxo-2*H*-chromen-7-yloxy) acetic acid

Scheme 1 illustrates the procedure to fabricate 2-(4-methyl-2-oxo-2*H*-chromen-7-yloxy) acetic acid (MCYAA). 17.8 g 7-hydroxy-4 methyl coumarin (HMC, 0.1 mol) and acetacetic ether (13.0 g, 0.1 mol) were added in 75 mL DMF. Then 19.8 g (0.2 mol) potassium acetate was added slowly with stirring. The reaction lasted for 24 h at 88 °C under a nitrogen atmosphere. The product was poured into 75 mL of ice water, and filtered to obtain the crude product. Finally, the crude product were recrystallized twice in ethyl acetate to obtain MCYAA. MCYAA was kept away from light for future use.

2.3. Preparation of PVA-*g*-HMC

PVA-*g*-HMC was synthesized by esterification reaction (Scheme 2). PVA (3.5 g) was completely dissolved in 50 mL DMF at 120 °C in a 150 mL three-neck round-bottom flask. After cooled down to 100 °C, the MCYAA (11.0 g, 0.05 mol) and *N*,*N*′-dicyclohexycarbodiimide (1 mL, as dehydrating agent) was added one-off under stirring. Then the catalyst dithio-butyl laurate was added drop-wise to the system. The reaction lasted for 24 h (at least) at 88 °C under a nitrogen atmosphere. The excess solvent in the system was removed by a rotary PVA porator. Finally, the crude product was extracted and purified by ethyl acetate, and dried in a vacuum at 60 °C for 24 h.

2.4. Preparation of control sample of PVA

A bottle of 10 mL water was heated at 98 °C and keep stirring at 300 rpm. 1 gram of PVA powder was added into water. After heating and stirring for 4 hours, the solution was coated on glass. After drying in a vacuum at 60 °C for 2 hour, control sample of PVA was got.

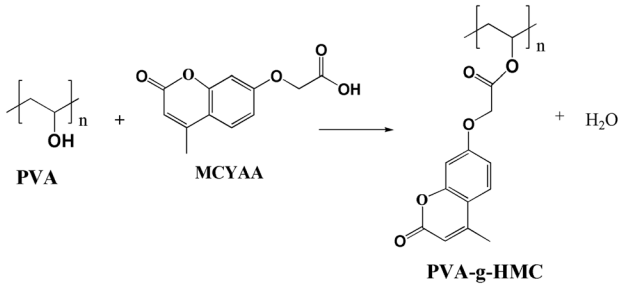

Scheme 2 The procedures to prepare PVA-*g*-HMC.

2.5. Characterizations

A ThermoFisher IS10 Fourier transformation infrared spectrometer was used to record fourier transform infrared (FT-IR) spectra. The spectra were obtained in the range of 4000–525 cm^{-1}. The number of scans was 32 at the resolution of 2 cm^{-1}. For the HMC and MCYAA, the samples were prepared by potassium bromide. While for the PVA and PVA-*g*-HMC samples were prepared in the form of films(0.20 mm thick) by a laminator (CHTECH, CH-0205, China).

^{1}H NMR spectra was measured by a VARIAN Mercury-Plus 300 (300 MHz) with dimethyl sulfoxide (DMSO-d6) as solvent.

Differential scanning calorimetry (DSC) measurements were tested by a TA Instruments DSC 2500 (at a heating rate of 10 °C min^{-1}, nitrogen purge). Since the thermal history of sample processing had a great influence on the formation of polymer crystals, we chose the second scan result of the DSC curve as the basis for discussion.

In order to test the affects of UV radiation on materials, TA Instruments DSC 2500 with UV curing system (UV-DSC) was also used for photo-calorimetric studies of the photo-reversible crosslinking resins. 0.20 mm thick sample films were irradiated by a UV light of 354 nm(60 W m^{-2}).

In order to study the photo-reversible crosslinking reaction of PVA-*g*-HMC. Film samples were firstly irradiated under an UV-light of 354 nm (15 mW cm^{-2}) to yield the crosslinked resin *via* photo-dimerization. Afterwards, UV-light was changed into 254 nm (15 mW cm^{-2}), allowing the photo-cleavage reaction of PVA-*g*-HMC to proceed. UV-Vis spectra of PVA-*g*-HMC which underwent photo-dimerization and photo-cleavage were recorded with a Hitachi 3900 UV vis spectrophotometer.

The crosslinking degrees (CR%) of PVA-*g*-HMC resin was tested by DMF extraction method (technically equivalent to the standard ISO 16152 and ASTM D5492) and calculated according to the following eqn (1):

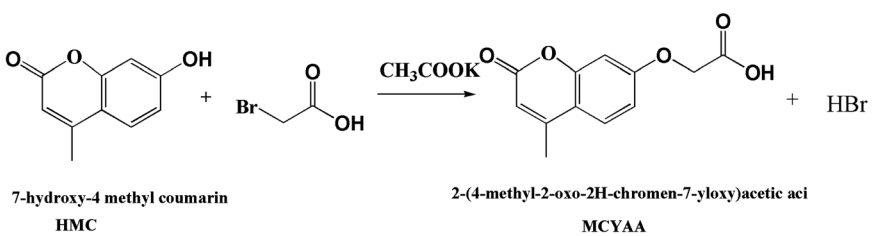

Scheme 1 The procedures to prepare 2-(4-methyl-2-oxo-2*H*-chromen-7-yloxy)acetic acid.

$$CR\% = (W_1 - W_2)/W_1 \times 100\% \quad (1)$$

In the equation, the W_1 was the weight of PVA-*g*-HMC resin before extraction, and W_2 was the weight of PVA resin after extraction.

For a quantitative description of the performance for AM, (1) the adhesion strength of PVA-*g*-HMC resin in glass/resin system were performed on a universal testing machine, model H10K-S (Hounsfield, the United Kingdom) according to ISO 8510-2 on at a crosshead speed of 5 cm min^{-1}. Each value obtained represented the average of nine samples. (2) The thermal conductivity were tested by a thermal conductivity tester (XIATECH, China). The sample size was at least 20 mm × 20 mm × 3 mm. (3) Oxygen transmission rate of PVA-*g*-HMC resin was performed on an oxygen permeability tester, model 2/21 MD (Mocon, United States of America). The test range (sample area 5 cm^2) of oxygen permeability tester was 1.0–2000 cm^3 per m^2 per day, and the testing repeatability was ± 0.05 cm^3 per m^2 per day.

The mechanical properties of the samples were tested on a SANS-CMT6103 electronic material universal testing machine, the tensile rate was 10 mm min^{-1}, the temperature was 23 ± 2 °C, and a 10 N sensor was used. PVA-*g*-HMC DMF solution was poured on the glass mold first. Then vacuum dried at 80 °C to remove the solvent, and form a film with a thickness of about 200 ± 25 μm in the glass mold. Placed the film on Rayonet In the RPR-100 ultraviolet light reactor, use 354 nm (15 mW cm^{-2}) ultraviolet light for 90 minutes to form a crosslinked structure, and use the double-sided irradiation method to maximize the coumarin in the film. Referring to ISO 527-3 "Test Conditions for Films and Sheets", use a dumbbell-shaped rubber cutter to cut the film into a standard dumbbell-shaped test piece with a length of 115 mm and a width of 6 mm.

3. Results and discussion

3.1. Synthesis of MCYAA

In order to carry out esterification successfully, coumarin was modified to MCYAA. The structure of MCYAA was confirmed by FTIR and ^{1}H NMR spectra. Fig. 1 showed the FTIR spectra. For HMC sample (Fig. 1a), the peaks at 3200 cm^{-1} suggests that –OH in the phenyl, while peak at 1670 cm^{-1} represents C=O of carbonyl. Meanwhile, peaks at 1240 cm^{-1}, 977 cm^{-1} and 840 cm^{-1} represents –O– in the epoxy ring. Significant change occurs in the FTIR spectrum of MCYAA (Fig. 1b) that peak of –OH in the carbonyl at 3540 cm^{-1} was presented. While the peaks of –O– in the epoxy ring represented at 1240 cm^{-1}, 977 $cm^{-1}$and 840 cm^{-1} and peak of C=O in the epoxy ring at 1670 cm^{-1} were retained. These changes indicated that HMC and acetacetic ether react under the catalytic of potassium acetate. NO oxidation and ring-opening reaction occurred during the synthesis of MCYAA.[13–19,27]

To further investigate the synthesis of MCYAA, ^{1}H NMR measurements were conducted. It could be observed from Fig. 2a that the protons of aromatic rings in HCM were found at 6.65 and 7.58 ppm, the protons of epoxy ring were found at 3.33 ppm, and the protons of –OH were observed at 10.48 ppm. While for samples of MCYAA (Fig. 2b), the protons of aromatic

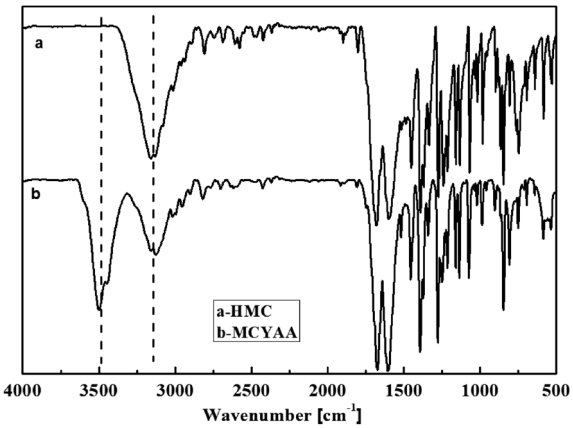

Fig. 1 FTIR spectrum of HMC (a) and MCYAA (b).

rings were found at 6.38 and 7.31 ppm, the protons of epoxy ring were found at 4.06 ppm, and the protons of –OH were observed at 10.21 ppm. Significant change occurred at 5.83 ppm which represents the protons of $–CH_2–O–$. In combination with the above results of FTIR, a conclusion could be drawn that MCYAA was synthesized successfully.[13–19,27,28]

3.2. Synthesis of PVA-*g*-HMC

PVA-*g*-HMC was synthesized by esterification reaction under the catalytic of dith-butyl dilaurate. FTIR and ^{1}H NMR were used to

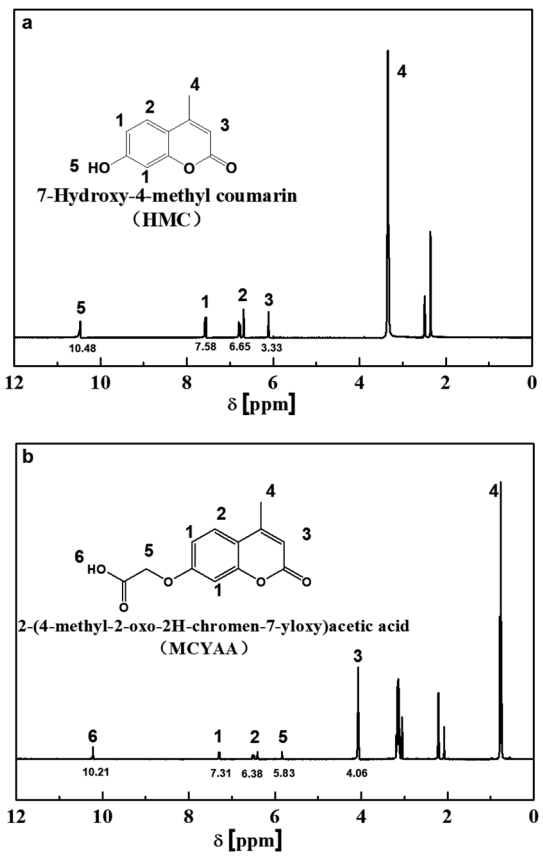

Fig. 2 ^{1}H NMR spectrum of HMC (a) and MCYAA (b).

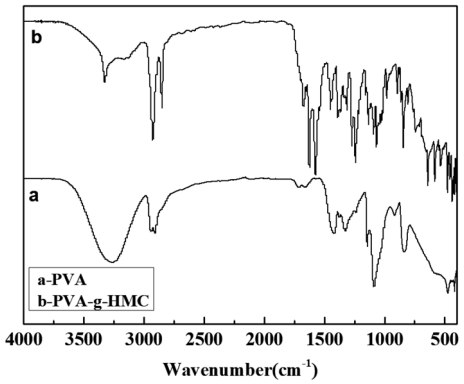

Fig. 3 FTIR spectrum of PVA (a) and PVA-*g*-HMC (b).

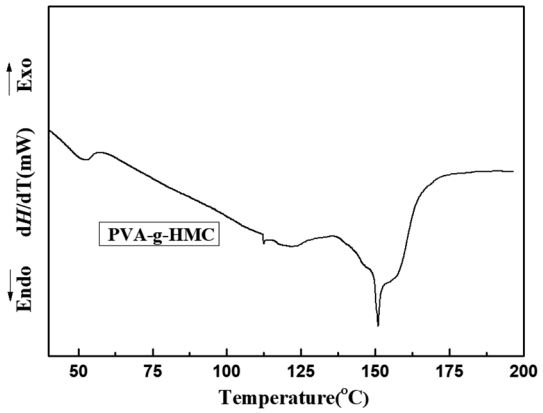

Fig. 5 DSC curves of PVA-*g*-HMC.

confirm the synthesis of PVA-*g*-HMC. The structure of PVA-*g*-HMC was confirmed by FTIR and NMR spectra. The FTIR spectra in Fig. 3 showed certain regular changes. For PVA, the two peaks at 1459 and 1333 cm^{-1} suggested that CH_2 in the backbone. The peak at 2930 cm^{-1} represented CH_2 in the backbone stretching vibrations absorption. And peak at 3250 cm^{-1} represented –OH in the backbone stretching vibrations absorption. For PVA-*g*-HMC, the most striking difference in PVA sample was the appearance of peak at 1700 cm^{-1} which represented ester C=O absorption (including the contribution of conjugative effect of phenyl) and that at 1630 cm^{-1} was related to the C=C of phenyl absorption.[12]

Fig. 4 showed results of ^{1}H NMR measurements. For sample of PVA(Fig. 4a), the protons of backbone were found at 1.23, 1.30 ppm, the protons of $–CH_2–OH$ were found at 3.33 ppm, and the protons of –OH were observed at 2.48 ppm. While for samples of PVA-*g*-HMC, characteristic peaks of HMC such as protons of aromatic rings at 6.77 and 7.62 ppm, the protons of epoxy ring at 6.22 ppm were found in the ^{1}H NMR spectrum of PVA-*g*-HMC. Therefore, a conclusion could be drawn that PVA-*g*-HMC was synthesized successfully by esterification reaction under the catalytic of dith-butyl dilaurate.[18]

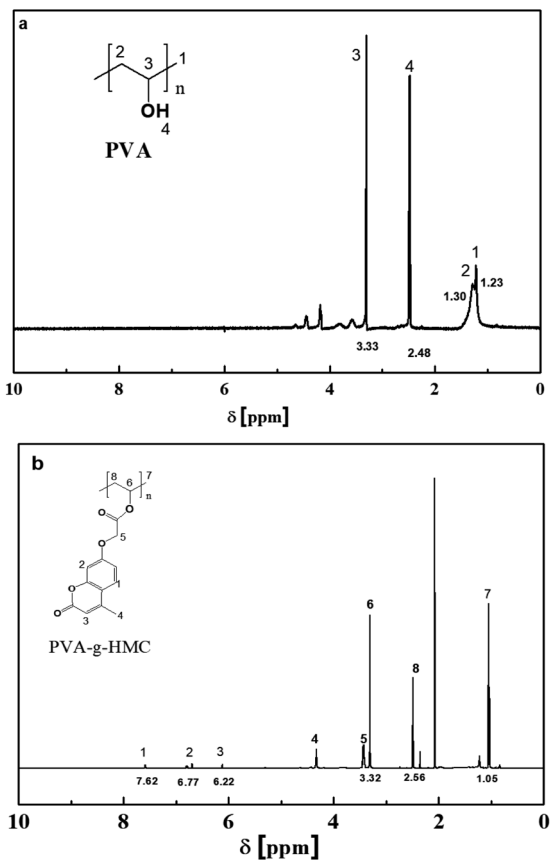

Fig. 4 ^{1}H NMR spectrum of PVA (a) and PVA-*g*-HMC (b).

3.3. Thermal analysis

The DSC melting endotherms corresponding to the heating scans for PVA-*g*-HMC was shown in Fig. 5. Concerning to the heating scan of PVA-*g*-HMC, the glass transition temperature was 52 °C. The melting endothermic peak was 150 °C. Some structural modification, like some crosslinking and chemical modifications, that could be taking place and affecting the crystallization process, indicating that the PVA-*g*-HMC had a good processing adaptability.[18,27]

3.4. Effect of temperature on photo-polymerization of PVA-*g*-HMC

In order to study the effect of temperature on photo-polymerization of PVA-*g*-HMC, the DSC curve of the sample under 354 nm ultraviolet irradiation was tested by UV-DSC, and the results were shown in Fig. 6. Previous studies showed that in order to obtain the photo-reversible crosslinking properties of polymers, it was necessary to give good mobility of coumarin groups in the polymer, so that the adjacent coumarin groups could collide with each other to produce photo-induced cross-linking reaction. This required that the temperature of PVA-*g*-HMC′ photo-polymerization must be above the glass transition temperature. The UV-DSC results show that the Tg of PVA-*g*-HMC was about 55 °C, so we choose two temperatures of 90 and 120 to irradiate the samples, and record the changes of the sample's thermal function. The curve on Fig. 6a showed the

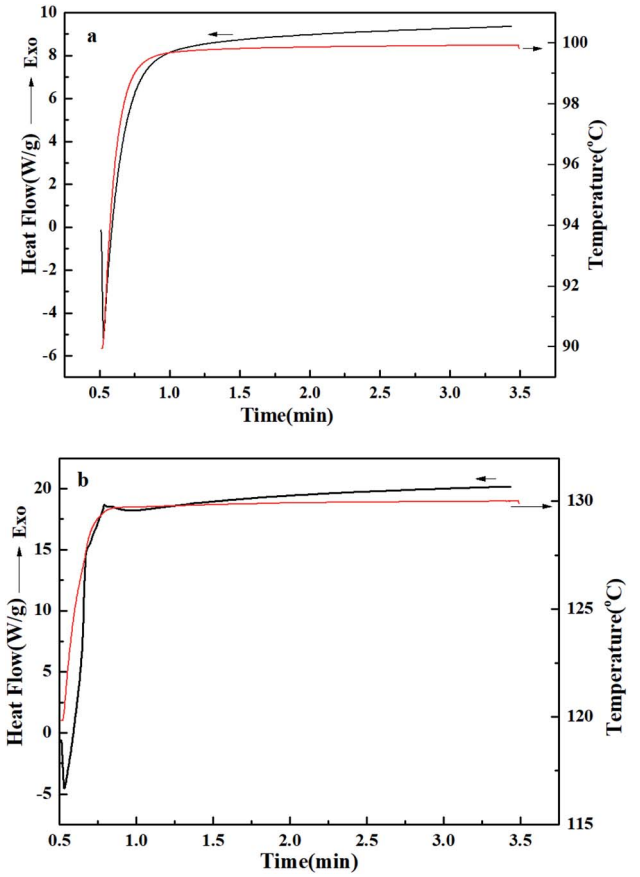

Fig. 6 UV-DSC curves of PVA-*g*-HMC at different temperatures: (a) at 130 °C, (b) at 140 °C.

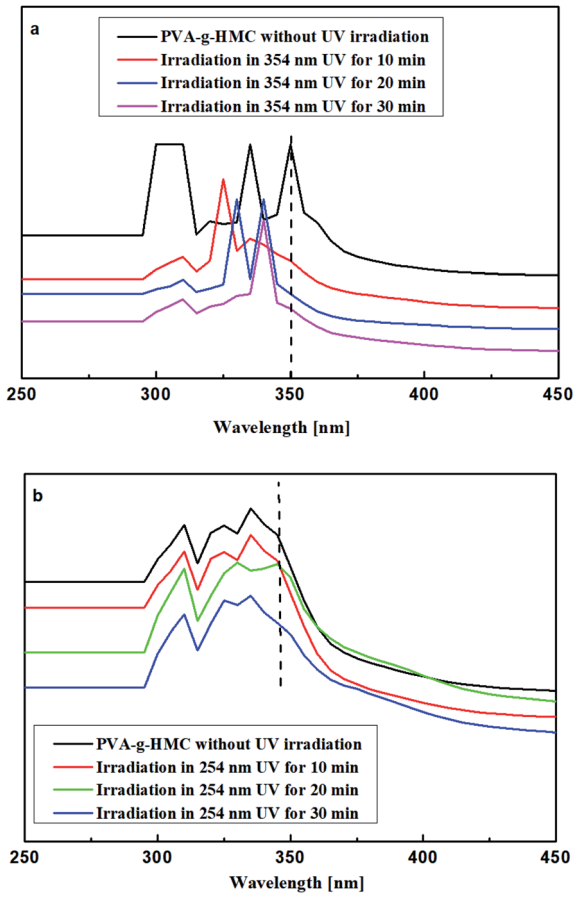

Fig. 7 UV-Vis spectra of PVA-*g*-HMC. (a) Photo-dimerization upon irradiation at 354 nm; (b) photo-cleavage upon irradiation at 254 nm.

result of PVA-*g*-HMC under UV irradiation at 90 °C. No exothermic peak, no photo-polymerization. However, we could see from Fig. 6b that the PVA-*g*-HMC was exothermic after ultraviolet irradiation. This is due to the photo-crosslinking reaction of HMC. Increasing the temperature was conducive to improving the mobility of coumarin group chain end. This result showed that the photo-crosslinking reaction of PVA-*g*-HMC had a high dependence on temperature. Raising the temperature was conducive to the photo-polymerization of PVA-*g*-HMC.

3.5. Photo-reversible crosslinking

Reversible photo-crosslinking behavior of PVA-*g*-HMC (DMF solution of PVA-*g*-HMC) was examined by UV-Vis spectroscopic analysis. Under UV-light irradiation of 354 nm, typical absorptions of coumarin appear (Fig. 7a): a π–π* transition between 300 and 354 nm was assigned to the pyrone nucleus. With the irradiation time rise, the absorption of samples at 354 nm decreased. This was due to the dimerization of double bonds in 4-methylcoumarin dimerize which form the cyclobutane rings (Scheme 3). The dimerization destroyed the conjugated p-system. Therefore, the absorbance at 354 nm could be used to quantitative analysis the dimerization degree of the 4-methylcoumarin moieties of PVA-*g*-HMC. Obviously, we could get this knot that the photo-crosslinking of PVA-*g*-HMC was realized under 354 nm UV irradiation for 10 min.[20–24]

When the UV-light source was changed into 254 nm (15.6 mW cm^{-2}), the dimerization degree rapidly decreased (Fig. 6b), which reflected in the reappear of absorption at 354 nm in Fig. 7b. Optical-cleavage of PVA-*g*-HMC was realized after 10 min irradiation of 254 nm UV light. Prolonged exposure did

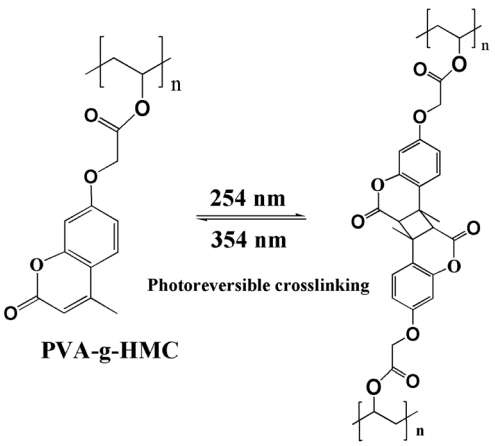

Scheme 3 Photo-reversible crosslinking mechanism of PVA-*g*-HMC.

Table 1 Crosslinking degree of PVA-*g*-HMC

	Reused times			
PVA-*g*-HMC samples	0	1	2	3
Irradiated by 354 nm UV for 10 min	66.2	60.2	56.1	50.3
Irradiated by 256 nm UV for 10 min	6.1	8.5	11.3	14.2

Table 2 Peeling strength of PVA-*g*-HMC

Samples	PVA	PVA-*g*-HMC
Peeling strength (N mm^{-1})	15.70 ± 3.12	14.79 ± 2.76

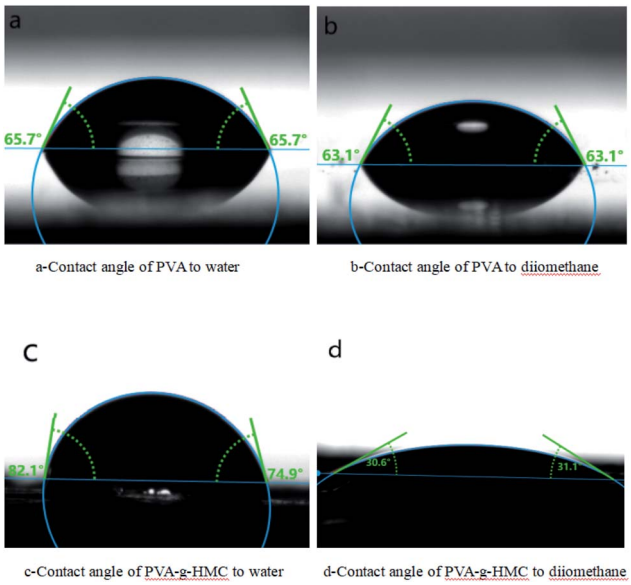

Fig. 8 Contact angle of PVA and PVA-*g*-HMC.

not affect the efficiency of photo-reversible but would result in an irreversibly crosslinked structure. Therefore, a reasonable irradiation time with 354 nm (photo-crosslink) or 254 nm UV light (photo-cleavage) of 10 min was critical for photo-reversible crosslinking of PVA-*g*-HMC.[20–24]

In order to further verify the photo-reversible crosslinking performance of PVA-*g*-HMC, *N*,*N*′-dimethylformamide (DMF) was used to extract the sample. The DMF extraction results of PVA-*g*-HMC samples of different reused times were shown in Table 1. It could be seen from the Table 1 that PVA-*g*-HMC undergoes dimerization reaction after UV irradiation at 354 nm, the crosslinking degree of the sample was 66.2%. Then the crosslinked sample was irradiated with 254 nm UV lamp, the crosslinking degree of the sample decreased to 6.1%. This result confirmed that some irreversible dimer configuration was produced in the process of photo-dimerization and crosslinking of PVA-*g*-HMC. After that, the samples were recycled. The crosslinking degree of the sample decreased with the increase of the times of repeated use, while the crosslinking degree of the photo-dimerized sample increases continuously. If the critical service condition was 60% crosslinking degree, the crosslinking degree of resin decreased greatly after reuse twice, which needs further improvement.

Table 3 Surface free energies of PVA and PVA-*g*-HMC

Materials	γ (mN m^{-1})	γ^d (mN m^{-1})	γ^p (mN m^{-1})
Glass	46.10	31.01	15.09
PVA	41.80	26.99	14.81
PVA-*g*-HMC	46.23	45.04	1.19

3.6. Adhesive performance

It's well known that high performance AM resins could retain its desirable mechanical, thermal, and chemical properties when subjected to harsh environment (such as high temperature, high pressure, and corrosive chemicals). Furthermore AM resins were required to have improved mechanical properties and functionality like thermal and electrical conductivity.

Table 2 showed the peel strength of PVA and PVA-*g*-HMC. The peel strength between the PVA resin and glass was 15.70 N mm^{-1}. For samples of PVA-*g*-HMC, the peel strength increases to 14.79 N mm^{-1}. Peel strength without much change could be attributed to the phenyl rings which were grafted onto the molecular chain lead PVA-*g*-HMC to a stronger polar polymer.

To verify the analysis from the viewpoint of thermodynamics, surface energies, γ, of the related materials was measured (Fig. 8, Table 3), in which γ^d and γ^p represent dispersion and polar parts, respectively.[29,30] Accordingly, work of adhesion, *W*, could be calculated from:

$$W_{AB} = 2\sqrt{\gamma_A^d \gamma_B^d} + 2\sqrt{\gamma_A^p \gamma_B^p} \quad (2)$$

where the subscripts A and B denote materials pair in contact. From the data in Table 3, the work of adhesion between glass and PVA was 87.75 mJ m^{-2}. While, the work of adhesion between glass and PVA-*g*-HMC was 83.23 mJ m^{-2}. Evidently, less energy has to be consumed when breaking the joint of glass/PVA-*g*-HMC apart, but there was not much difference in adhesive performance.

3.7. Thermal conductivity

The thermal properties of the material arguably played one of the most important roles in additive manufacturing. These properties dictated the rate of solidification, amongst other things, which in turn controls the phase composition and the mechanical properties. While there was, for the most part, sufficient published empirical data on the thermal properties of the common materials used in AM, the thermal properties of these materials were rarely powder like, especially in sintered or melted state. There was a need for accurate AM thermal property data. Table 4 showed the thermal conductivity of PVA and PVA-*g*-HMC. The thermal conductivity of PVA was 0.21 W m^{-1} K^{-1}. Heat transfer physics described the kinetics of energy storage, transport, and transformation by principal energy

Table 4 Thermal conductivity of PVA-*g*-HMC

Samples	PVA-*g*-HMC (uncrosslinked)	PVA-*g*-HMC (crosslinked)
Thermal conductivity ($W\ m^{-1}\ K^{-1}$)	0.2167 ± 3.01	0.2436 ± 2.31

Table 5 Oxygen transmission rate of PVA-*g*-HMC

Samples	PVA	PVA-*g*-HMC (uncrosslinked)	PVA-*g*-HMC (crosslinked)
Oxygen transmission rate (cm^3 per m^{-2} per day)	2.53	2.91	2.76

Table 6 Tensile performance of PVA-*g*-HMC

	Uncrosslinked PVA-*g*-HMC		Crosslinked PVA-*g*-HMC	
Samples	Mean	Std deviation	Mean	Std deviation
Tensile trength (MPa)	15.36	1.22	16.91	1.15

carriers: phonons (lattice vibration waves), electrons, fluid particles and photons. Compare with the molecular structure of PVA, phenyl rings were grafted to the molecular chain of PVA-*g*-HMC, which were the carriers for heat transformation. However, spaced phenyl rings were difficult to form an effective electronic transmission channel to obtain an excellent thermal performance. Therefore, the thermal conductivity of PVA-*g*-HMC with 0.24 $W\ m^{-1}\ K^{-1}$ was slightly higher than that of PVA.[31–33]

3.8. Barrier performance

PVA film was nontoxic and harmless. It had excellent barrier to hydrogen, oxygen and carbon dioxide. In addition, it had good oil resistance, solvent resistance, high moisture permeability, anti-static and good printability. It played an important role in barrier membrane materials.[34–37] However, the melting temperature (above 220 °C) of PVA was close to the decomposition temperature(above 230–250 °C), so it was difficult to thermoplastic processing. Oxygen transmission rate of PVA and PVA-*g*-HMC were shown on Table 5. Due to semi-crystallization as well as the role of intermolecular hydrogen bonds, PVA had an excellent barrier property against oxygen, of which the oxygen transmission rate was 2.53 cm^3 per m^{-2} per day. The oxygen transmission rate decreased due to low crystallization and the role of inter-molecular hydrogen bonds after grafting reaction. Since incompletely grafted, the role of intermolecular hydrogen bonds in PVA-*g*-HMC remained, reflecting on the oxygen transmission rate was 2.91 cm^3 per m^{-2} per day. Furthermore, crosslinking improved the barrier properties of the polymer. An oxygen transmission rate of 2.76 cm^3 per m^{-2} per day was got for crosslinked PVA-*g*-HMC. That means that the strong hydrogen bond between PVA molecules was weakened and the crystallization of PVA was inhibited. This lead to the reduction of PVA's oxygen barrier performance. However, the decrease of its melting point was beneficial to its melting process. After crosslinking, the oxygen barrier property of PVA-*g*-HMC was improved, which makes the material useful in the field of barrier membranes.

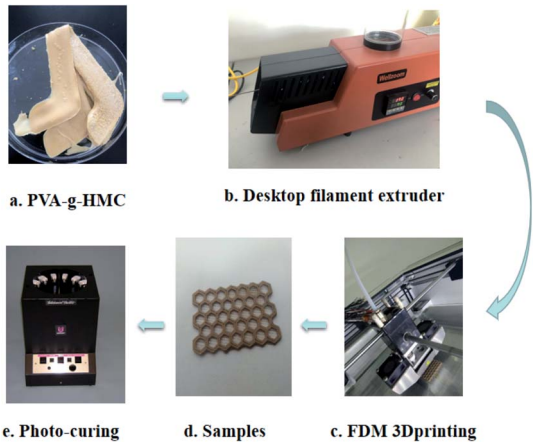

Fig. 9 Application of PVA-*g*-HMC in additive manufacturing.

3.9. Tensile performance

In the study, we also compared the tensile strength of PVA-*g*-HMC before and after UV irradiation. The test result was the average of five repeated tests. According to the test results in Table 6, the tensile trength of uncrosslinked PVA-*g*-HMC was 15.36 MPa. While for the sample of crosslinked PVA-*g*-HMC was 16.91 MPa. This showed that PVA-*g*-HMC had better mechanical properties, and UV crosslinking could improve the mechanical properties of the resin.

3.10. Application in additive manufacturing

The compounds (Fig. 9a) were added into a desktop filament extruder (Fig. 9b) to made of 3D printing wires. This wires was used directly for FDM 3D printing (Fig. 9c). In the FDM processes, PVA-*g*-HMC wires were heated to 170 °C and extruded through a procedure-controlled nozzle: materials were deployed layer by layer on the printing surface in a warm up plate (Fig. 9d). Finally, the photo-curing of samples were occurred by a photo-chemical reactor for photo-curing (Fig. 9e).

The composites developed in this study demonstrate a number of advantages, including low cost and excellent overall performances, opening any number of opportunities for application in additive manufacturing.

4. Conclusions

The new type of PVA-*g*-HMC resin proves to be able to photo-reversible crosslinking under the irradiation of different

ultraviolet. Synthesis of PVA-*g*-HMC was analyzed by FTIR and ^{1}H NMR that the target product was synthesized successfully. TGA and DSC analysis showed that the T*m* of PVA-*g*-HMC was about 150 °C, which had a good processing adaptability than PVA. The photo-reversible crosslink was proved feasible and the reversible condition was optimized by UV-Vis spectroscopic analysis. A reasonable irradiation time with 354 nm (crosslink) or 254 nm UV light (cleavage) of 10 min was critical for photo-reversible crosslinking of PVA-*g*-HMC. Performances of PVA-*g*-HMC for AM resin were also investigated. The experimental results indicated that PVA-*g*-HMC has better adhesion property (14.79 N mm^{-1}), thermal conductivity (0.24 W m^{-1} K^{-1}) and oxygen barrier performance (2.76 cm^3 per m^{-2} per day). On the whole, both processability and performance of the PVA-*g*-HMC resin meet the requirements of practical applications.

Author contributions

Conceptualization, X. L. and Q. L.; methodology, H. X. and J. X.; formal analysis, X. L. and Q. L.; writing—original draft preparation, H. X.; writing—review and editing, J. X. and Q. L.; funding acquisition, H. X and Q. L. All authors had read and agreed to the published version of the manuscript.

Funding

This work is financially supported by National Natural Science Foundation of China (Grant No. 51703090), Cultivation Plan for Outstanding Young Talents of Fujian Province (Grant No. 3230412501), Fuzhou Municipal Science Foundation (Grant: 2019-G-57), Fuzhou Municipal Science Foundation (Grant: 2020-GX-2).

Conflicts of interest

The authors declare no conflict of interest.

Acknowledgements

This work was supported by Fujian Engineering and Reaearch Center of New Chinese Lacquer Materials.

References

1 X. Wang, M. Jiang, Z. W. Zhou, J. . h. Gou and D. Hui, 3D printing of polymer matrix composites: A review and prospective, *Compos. B Eng.*, 2017, **110**, 442–458, DOI: 10.1016/j.compositesb.2016.11.034.

2 A. Munaz, R. K. Vadivelu, J. S. John, M. Barton, H. Kamble and N. T. Nguyen, Three dimensional printing of biological matters, *J. Sci. Adv. Mat. Dev.*, 2016, **1**, 1–17, DOI: 10.1016/j.jsamd.2016.04.001.

3 A. D. Gianni, R. Bongiovanni, S. Turri, F. Deflorian, G. Malucelli and G. Rizza, UV-cured coatings based on waterborne resins and SiO2 nanoparticles, *J. Coa. Technol. Res.*, 2009, **6**, 177–185, DOI: 10.1007/s11998-008-9137-1.

4 Y. S. Khoo, T. M. Walsh, M. W. Timothy, F. Lu and A. G. Aberle, Method for quantifying optical parasitic absorptance loss of glass and encapsulant materials of silicon wafer based photovoltaic modules, *Sol. Energ. Mat. Sol. C.*, 2012, **12**, 153–158, DOI: 10.1016/j.solmat.2012.03.00.

5 J. Liu, L. Sun, W. Xu, Q. Wang, S. Yu and J. Sun, Current advances and future perspectives of 3D printing natural-derived biopolymers, *Carbohyd. Polym.*, 2019, **207**, 297–316, DOI: .

6 E. Trovatti, T. M. Lacerda, A. J. F Carvalho and A. Gandini, Recycling tires? Reversible crosslinking of poly(butadiene), *Adv. Mat.*, 2015, **27**, 2242–2245, DOI: 10.1002/adma.201405801.

7 M. He, Y. Zhao, Y. Liu and D. Wei, A 3D printable self-healing composite conductive polymer for sensitive temperature detection, *Chinese. Chem. Lett.*, 2019, **6**, DOI: 10.1016/j.cclet.2019.06.003, Available online. .

8 R. Calderón-Villajos, A. J. López, L. Peponi, J. Manzano-Santamaría and A. Ureña, 3D-printed self-healing composite polymer reinforced with carbon nanotubes, *Mater. Lett.*, 2019, **249**, 91–94, DOI: 10.1016/j.matlet.2019.04.069.

9 Z. H. Lu and Q. Yao, Energy analysis of silicon solar cell modules based on an optical model for arbitrary layers, *Sol. Energy*, 2007, **81**, 636–647, DOI: 10.1016/j.solener.2006.08.014.

10 H. S. Nam, W. J. Lee, S. H. Cha and K. J. Lee, Polymeric micropowders from thermal reversible crosslinking of oligomers, *Adv Powder Technol*, 2019, **30**, 2580–2587, DOI: 10.1016/j.apt.2019.08.005.

11 Q. Fu, L. Cheng, Y. Zhang and W. Shi, Preparation and reversible photo-crosslinking/photo-cleavage behavior of 4-methylcoumarin functionalized hyperbranched polyester, *Polymer*, 2008, **49**, 4981–4988, DOI: 10.1016/j.polymer.2008.09.017.

12 J. P. Chesterman, T. C. Hughes and B. G. Amsden, Reversibly photo-crosslinkable aliphatic polycarbonates functionalized with coumarin, *Eur. Polym. J.*, 2018, **105**, 186–193, DOI: 10.1016/j.eurpolymj.2018.05.038.

13 C. Salgado, M. P. Arrieta, M. Fernández-García and D. López, Silica-nanocomposites of photo-crosslinkable poly(urethane)s based on poly(ε-caprolactone) and coumarin, *Eur. Polym. J.*, 2017, **93**, 21–32, DOI: 10.1016/j.eurpolymj.2017.05.030.

14 J. Manhart, S. Ayalur-Karunakaran, S. Radl, A. Oesterreicher and S. Schlögl, Design and application of photo-reversible elastomer networks by using the [4πs+4πs] cycloaddition reaction of pendant anthracene groups, *Polymer*, 2016, **102**, 10–20, DOI: 10.1016/j.polymer.2016.08.106.

15 L. López-Vilanova, I. Martinez, T. Corrales and F. Catalina, Photoreversible crosslinking of poly-(ethylene-butyl-acrylate) copolymers functionalized with coumarin chromophores using microwave methodology, *Reac Funct Polymers*, 2014, **85**, 28–35, DOI: 10.1016/j.reactfunctpolym.2014.10.001.

16 C. Salgado, P. M. Arrieta, L. Peponi, D. López and M. Fernández-García, Photo-crosslinkable polyurethanes reinforced with coumarin modified silica nanoparticles for photo-responsive coatings, *Prog. Org. Coat.*, 2018, **123**, 63–74, DOI: 10.1016/j.porgcoat.2018.06.019.

17 R. Beninatto, C. Barbera, O. De Lucchi, G. Borsato and N. Elvassore, Photocrosslinked hydrogels from coumarin derivatives of hyaluronic acid for tissue engineering applications, *Mat. Sci. Eng: C.*, 2019, **96**, 625–634, DOI: 10.1016/j.msec.2018.11.052.

18 S. R. Govindarajan, T. Jain, J. W. Choi, A. Joy and K. Vorvolakos, A hydrophilic coumarin-based polyester for ambient-temperature initiator-free 3D printing: Chemistry, rheology and interface formation, *Polymer*, 2018, **152**, 9–17, DOI: 10.1016/j.polymer.2018.06.014.

19 M. Eswaran, B. N. Sunil, N. Zainab and H. Gurumurthy, Synthesis, liquid crystalline properties and photo switching properties of coumarin-azo bearing aliphatic chains: Application in optical storage devices, *J. Mol. Liq.*, 2019, **292**, 111328, DOI: 10.1016/j.molliq.2019.111328.

20 R. S. Rivero, P. B. Solaguren, K. G. Zubieta and G.-J. A. Marcos- Fernándezb, A. Synthesis and characterization of photo-crosslinkable linear segmented polyurethanes based on coumarin, *Eur. Polym. J.*, 2017, **92**, 263–274, DOI: 10.1016/j.eurpolymj.2017.05.016.

21 G. Ciamician and P. Silber, Chemische lichtwirkungen. XXIII, *Ber. Dtsch. Chem. Ges.*, 1912, **45**, 1540–1546, DOI: 10.1002/cber.19120450215.

22 C. Krauch, S. Farid and G. O. Schenck, Photo-C4-cyclodimerisation von cumarin, *Chem. Ber.*, 1966, **99**, 625–633, DOI: 10.1002/cber.19660990237.

23 H. Morrison, H. Curtis and T. M. McDowell, Solvent effects on the photodimerization of coumarin, *J. Am. Chem. Soc.*, 1966, **88**, 5415–5419, DOI: 10.1021/ja00975a009.

24 R. Hoffman, P. Wells and H. Morrison, Organic Photochemistry. XII. Further Studies on the mechanism of coumarin photodimerization. Observation of an unusual "Heavy Atom" Effect, *J. Org. Chem.*, 1971, **36**, 102–108, DOI: 10.1021/jo00800a022.

25 M. D. Cohen and G. M. J. Schmidt, Topochemistry. Part I. A survey, *J. Chem. Soc.*, 1964, 1996–2000.

26 A. Duval, H. Lange, M. Lawokom and C. Crestini, Reversible crosslinking of lignin via the furan-maleimide Diels-Alder reaction, *Green Chem.*, 2015, **17**, 4991–5000, DOI: 10.1039/C5GC01319D.

27 S. Y. Kim, T. H. Lee, Y. Park, J. H. Nam, S. M. Noh, I. W. Cheong and J. C. Kim, Influence of material properties on scratch-healing performance of polyacrylate graft polyurethane ethane network that undergo thermally reversible crosslinking, *Polymer*, 2017, **128**, 135–146, DOI: 10.1016/j.polymer.2017.09.021.

28 J. Ling, M. Z. Rong and M. Q. Zhang, Coumarin imparts repeated photochemical remediability to polyurethane, *J. Mater. Chem.*, 2011, **21**, 18373, DOI: 10.1039/C1JM13467A.

29 D. K. Owens and R. C. Wendt, Estimation of the surface free energy of polymers, *J. Appl. Polym. Sci.*, 1969, **13**, 1741–1747, DOI: 10.1002/app.1969.070130815.

30 E. E. Kahveci and T. Imdat, Experimental study on performance evaluation of PEM fuel cell by coating bipolar plate with materials having different contact angle, *Fuel*, 2019, **253**, 1274–1281, DOI: 10.1016/j.fuel.2019.05.110.

31 J. J. Park and K. G. Yoon, Thermal and mechanical properties of epoxy/Micro- and nano- mixed silica composites for insulation materials of heavy electric equipment, *IEEJ. T. Electr. Electr.*, 2011, **2**, 98–101, DOI: 10.4313/TEEM.2011.12.3.98.

32 T. Rettelbach, J. Sauberlich, S. Korder and J. Fricke, Thermal conductivity of silica aerogel powders at temperatures from 10 to 275 K, *J. Non-Cryst. Solids*, 1995, **186**, 278–284, DOI: 10.1016/0022-3093(95)00051-8.

33 A. Allahverd, M. Ehsani, H. Janpour and S. Ahmadi, The effect of nanosilica on mechanical, thermal and morphological properties of epoxy coating, *Pro. Org. Coat.*, 2012, **75**, 543–548, DOI: 10.1016/j.porgcoat.2012.05.013.

34 E. Espinosa, I. Bascón-Villegas, A. Rosal, F. Pérez-Rodríguez, G. Chinga-Carrasco and A. Rodríguez, PVA/(ligno) nanocellulose biocomposite films. Effect of residual lignin content on structural, mechanical, barrier and antioxidant properties, *Int. J. Bio. Macromol.*, 2019, **141**, 197–206, DOI: 10.1016/j.ijbiomac.2019.08.262.

35 X. Zhang, W. Liu, W. Liu and X. Qiu, High performance PVA/lignin nanocomposite films with excellent water vapor barrier and UV-shielding properties, *Int. J. Bio. Macromol.*, 2020, **142**, 551–558, DOI: 10.1016/j.ijbiomac.2019.09.129.

36 N. E. Kochkina and O. A. Butikova, Effect of fibrous TiO2 filler on the structural, mechanical, barrier and optical characteristics of biodegradable maize starch/PVA composite films, *Int. J. Bio. Macromol.*, 2019, **139**, 431–439, DOI: 10.1016/j.ijbiomac.2019.07.213.

37 H. Lee, J. You, H. Jin and H. W. Kwak, Chemical and physical reinforcement behavior of dialdehyde nanocellulose in PVA composite film: A comparison of nanofiber and nanocrystal, *Carbohyd. Polym.*, 2020, **232**, 115771, DOI: 10.1016/j.carbpol.2019.115771.